INTERNATIONAL JOURNAL OF HYPERTHERMIA
2021, VOL. 38, NO. 1, 393–401
https://doi.org/10.1080/02656736.2021.1875061

Experimental model of occluded biliary metal stent recanalization using irreversible electroporation via a tubular catheter

T. Rohan[a], T. Andrasina[a], T. Juza[a], P. Matkulcik[a], D. Červinka[b], I. Svobodova[c], V. Novotná[b], V. Bernard[d], V. Valek[a] and S. Nahum Goldberg[e]

[a]Department of Radiology and Nuclear Medicine, University Hospital Brno and Masaryk University Brno, Brno, Czech Republic; [b]Faculty of Electrical Engineering and Communication, Department of Power Electrical and Electronic Engineering, Brno University of Technology, Brno, Czech Republic; [c]Department of Pathology, St. Anne's University Hospital Brno, Brno, Czech Republic; [d]Faculty of Medicine, Department of Biophysics, Masaryk University, Brno, Czech Republic; [e]Medical Center, Hadassah Hebrew University, Jerusalem, Israel

ABSTRACT

Purpose: To demonstrate the feasibility of irreversible electroporation (IRE) for treating biliary metal stent occlusion in an experimental liver model.

Methods and materials: IRE was performed using an expandable tubular IRE-catheter placed in nitinol stents in the porcine liver. A 3-electrode IRE-catheter was connected to an IRE-generator and one hundred 100μs pulses of constant voltage (300, 650, 1000, and 1300 V) were applied. Stent occlusion was simulated by insertion of liver tissue both *ex vivo* ($n = 94$) and *in vivo* in 3 pigs ($n = 14$). Three scenarios of the relationship between the stent, electrodes, and inserted tissue (double contact, single contact, and stent mesh contact) were studied. Electric current was measured and resistance and power calculated. Pigs were sacrificed 72 h post-procedure. Harvested samples (14 experimental, 13 controls) underwent histopathological analysis.

Results: IRE application was feasible at 300 and 650 V for the single and double contact setup in both *ex vivo* and *in vivo* studies. Significant differences in calculated resistance between double contact and single contact settings were observed (*ex-vivo* $p < 0.0001$, *in-vivo* $p = 0.02$; Mann–Whitney). A mild temperature increase of the surrounding liver parenchyma was noted with increasing voltage (0.9–5.9 °C for 300–1000 V). The extent of necrotic changes in experimental samples *in vivo* correlated with the measured electric current ($r^2 = 0.39$, $p = 0.01$). No complications were observed during or after the *in-vivo* procedure.

Conclusion: Endoluminal IRE using an expandable tubular catheter in simulated metal stent occlusion is feasible. The relationship of active catheter electrodes to stent ingrowth tissue can be estimated based on resistance values.

ARTICLE HISTORY
Received 11 October 2020
Revised 4 January 2021
Accepted 7 January 2021

KEYWORDS
Irreversible electroporation; metal stent occlusion; metal stent recanalization; experimental model; thermocamera

Introduction

Survival of patients with cholangiocarcinoma has been improved to frequently exceed 12 months if current comprehensive oncologic treatment is employed [1,2]. This often includes the use of metal stents which are recommended for malignant biliary obstruction when survival expectancy is greater than 3 months [3]. However, the patency rate of biliary metal stents is challenging – reportedly lasting between 14 and 321 days [4–6]. Therefore, stent occlusion is a serious problem affecting the quality of life, morbidity, and mortality of patients undergoing palliative biliary procedures. Occlusion of metal stents is associated with epithelial hyperplasia, tumor ingrowth and overgrowth, dislocation, debris formation, and clot accumulation [7,8].

There are several methods reported for treating biliary metal stent occlusion, but none have shown satisfactory long-term results. Mechanical balloon cleaning is the simplest way of recanalization. However, it shows minimal effectiveness in cases of hyperplasia or tumor ingrowth [8,9]. Brachytherapy has been shown to be effective for the prevention of mucosal hyperplasia and tumor ingrowth before stent placement [10], but it is not widely adopted for the treatment of stent occlusion. Other solutions have included stent-in-stent placement or endoluminal radiofrequency ablation [5,11,12]. Endoluminal thermal ablation can be used for debulking and tumor growth deceleration, and potentially for biliary metal stent recanalization. For example, applying radiofrequency ablation using specialized bipolar catheters prior to metal stent insertion has shown increased survival and stent patency in small retrospective studies [13,14]. Yet, larger prospective studies are needed to confirm this. Regardless, the use of endoluminal thermal ablation is limited by the risk of bile duct injury in case of excessive

CONTACT T. Andrasina andrasina.tomas@fnbrno.cz Department of Radiology and Nuclear Medicine, University Hospital Brno and Masaryk University Brno, Jihlavská 20, Brno 625 00, Czech Republic

Supplemental data for this article can be accessed here.

heating of the metal stent which can become an active electrode [15].

Irreversible electroporation (IRE) is a relatively novel method for the percutaneous treatment of hepatic tumors [16]. IRE causes cell death and necrosis through cell membrane porosity induced by high-voltage microsecond pulses delivered to the tissue. The major touted benefits compared to thermal ablation is IRE's potential low heat production with ablation shape and volume being independent of thermal conductivity and loss, with effects directed on cellular membranes affording relative sparing of bile ducts and blood vessels [17]. Yet, IRE is no longer considered a solely non-thermal ablation method as prior experiments have demonstrated that temperature production during IRE linearly correlates with delivered energy to the point that thermal coagulation can be observed at high IRE doses [17]. Moreover, IRE is highly susceptible to changes in local electrical conductivity – something that is likely to occur in the presence of metallic hardware [18].

It is currently unclear whether irreversible electroporation can be performed safely and effectively in proximity to metal stents [19,20] and whether IRE using a dedicated tubular catheter has the potential to recanalize partially occluded or occluded metal stent. Accordingly, the primary goal of our study is to demonstrate the feasibility of endoluminal IRE applied via tubular catheters in partially occluded metal stents. The secondary endpoints are to determine feasible voltage settings for endoluminal usage of tubular IRE catheter and whether differences in electrical parameters (i.e., resistance and current) enable the determination of the number of active electrodes in contact with the stent mesh or the tissue occluding the stent (i.e., the relation of the catheter and ingrowth tissue within the stent).

Material and methods

Experiments were performed in two phases using *ex vivo* and *in vivo* liver models. The purpose of the initial *ex vivo* studies was to find an upper threshold for IRE in the metal stent and correlate it with macroscopically visible coagulation necrosis in proximity to IRE electrodes and thermal changes close to the mesh of metal stents. Based upon the results from the *ex vivo* study, promising scenarios were further recreated in an *in vivo* setting. The study design is visualized in Figure 1.

Equipment and IRE setting

For all experiments, thin liver tissue bands were inserted into bare-metal stents (nitinol 10x80mm, EGIS, S&G Biotech Inc., South Korea), to simulate in-stent occlusion. An experimental tubular 3 electrode IRE catheter (12 F expandable catheter, Ella CS, Czech Republic) was inserted into these partially occluded stents. The size of inserted liver tissue bands represented the maximal size of tissue that fit into the stent together with the catheter. The catheter was connected to an IRE generator, with two of three built-in electrodes set as active. IRE energy was delivered by a generator prototype

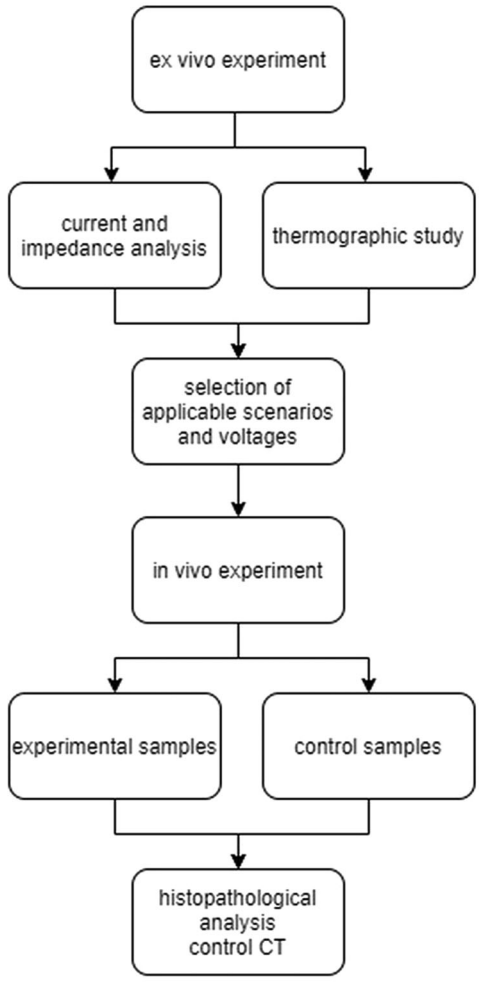

Figure 1. Flowchart demonstrating the design of the experiment.

constructed by the [redacted to maintain the integrity of the review process] [21]. IRE pulses were delivered to two active electrodes using clinically relevant parameters previously validated in experimental studies [18,22,23]. These included: DC voltage of 300, 650, 1000 and 1300 V, pulse length of 100 μs, 100 rectangular pulses with a repetition rate of 1 Hz. The self-expanding stent-shaped IRE catheter creates an approximately parallel position of the electrodes and the metal stent, inducing a nearly homogeneous electrical field. Average current values visualized on the oscilloscope during the IRE procedure were recorded. The average current of a given IRE procedure was calculated from the mean current amplitude of each IRE pulse. The resistance was calculated by Ohm's law from the voltage set on the IRE generator and the current visualized on the oscilloscope record. For simplicity, the resistance values of the metal parts of the electrical circuit were neglected when calculating the electrical intensity.

Experimental scenarios

The extent of two different degrees of stent occlusion were modeled: occlusion of more than 50% circumference of the lumen when both active electrodes were in contact with inserted tissue (scenario A – 'double electrode contact'), and

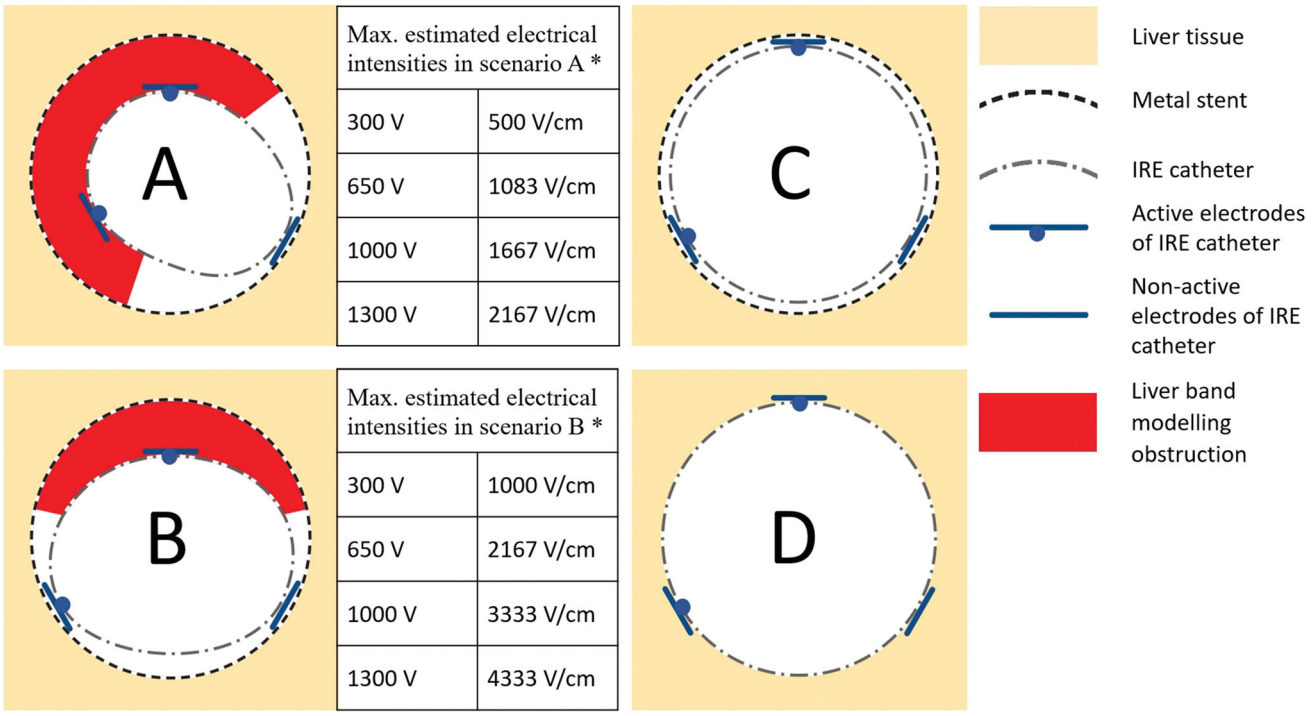

Max. estimated electrical intensities in scenario A *	
300 V	500 V/cm
650 V	1083 V/cm
1000 V	1667 V/cm
1300 V	2167 V/cm

Max. estimated electrical intensities in scenario B *	
300 V	1000 V/cm
650 V	2167 V/cm
1000 V	3333 V/cm
1300 V	4333 V/cm

Figure 2. Schematic depiction of experimental scenarios. Scenario A (double electrode contact) – tubular IRE catheter in metal stent, both active electrodes are in contact with inserted liver tissue; Scenario B (single electrode contact) – tubular IRE catheter in metal stent, with just one active electrode in contact with inserted liver tissue (the second electrode in contact with metal stent mesh); Scenario C (no occlusion) – tubular IRE catheter in metal stent, both active electrodes are in contact with the metal stent mesh; Scenario D – tubular IRE catheter surrounded by liver tissue (control). *In scenarios A and B, maximal estimated electrical intensities between active electrodes were calculated for 3 mm thick liver tissue localized between the metal stent and the IRE catheter.

occlusion of less than 50% circumference of the lumen, when just one active electrode was in contact with inserted tissue (scenario B – 'single electrode contact') (Figure 2). The severity of stricture in scenarios A and B ranged from 20 to 40% based upon the thickness of the inserted liver tissue (3 ± 1 mm). The estimated maximal uncorrected electrical intensities at a distance of 3 mm between the IRE electrodes and the metal stent were 500 V/cm at 300 V, 1083 V/cm at 650 V, 1667 V/cm at 1000 V and 2167 V/cm at 1300 V in scenario A, and 1000 V/cm at 300 V, 2167 V/cm at 650 V, 3333 V/cm at 1000 V and 4333 V/cm at 1300 V in scenario B. Two additional scenarios representing controls were performed *ex vivo*: scenario C – where both active electrodes were in direct contact with the metal stent; and scenario D – where IRE was applied directly into the liver groove with no stent present (Figure 2). Scenario C can be used to determine the resistance value of the metal parts of the circuit for the purpose of correcting the voltage in the tissue.

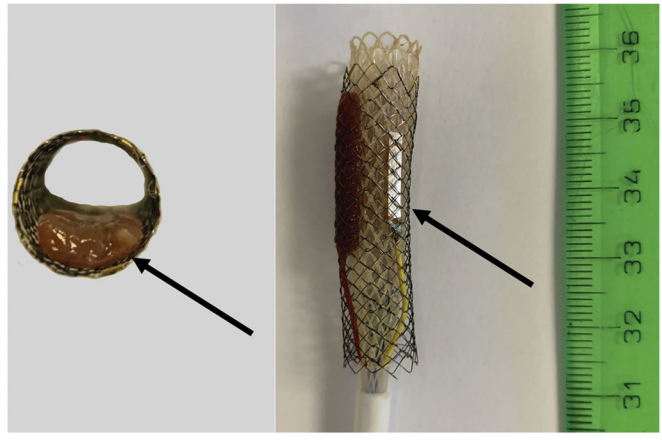

Figure 3. Model of metal stent with partial occlusion: Left – axial view of the metal stent with inserted band liver tissue (arrow). Right – tubular IRE catheter inside the metal stent with an inserted band of liver tissue between the stent and active IRE electrode (not visible), the other active electrode is in contact with the metal stent (visible arrow) (Scenario B).

Ex vivo experiments

Fresh porcine livers were used at room temperature (22 °C). Metal stents were inserted into scalpel-cut grooves in blocks of liver tissue (size 50 ± 10 mm) at a depth of 20 ± 5 mm. The bare portions of the metal stents were covered by at least 1 cm of liver tissue. Metal stent occlusion was modeled by inserting thin (3 ± 1 mm) tissue bands of liver into the lumen of the stent (Figure 3).

In total, 94 IRE procedures were performed: 35 each for Scenarios A (double electrode contact) and B (single electrode contact) with 10 procedures at 300 V, 650 V, 1000 V, and 5 procedures at 1300 V; 12 in Scenario C (stent mesh contact; 3 procedures at 300 V, 650 V, 1000 V, and 1300 V), and 12 in Scenario D (direct liver application; 3 procedures at 300 V, 650 V, 1000 V, and 1300 V). The number of scenarios was determined based upon performing a power analysis after 3 initial experiments in each scenario and voltage (95% power, statistical significance 0.05). Scenarios C and D served as controls. Given a very low standard deviation, 3 experiments at each of 300, 650, 1000 and 1300 V were considered sufficient.

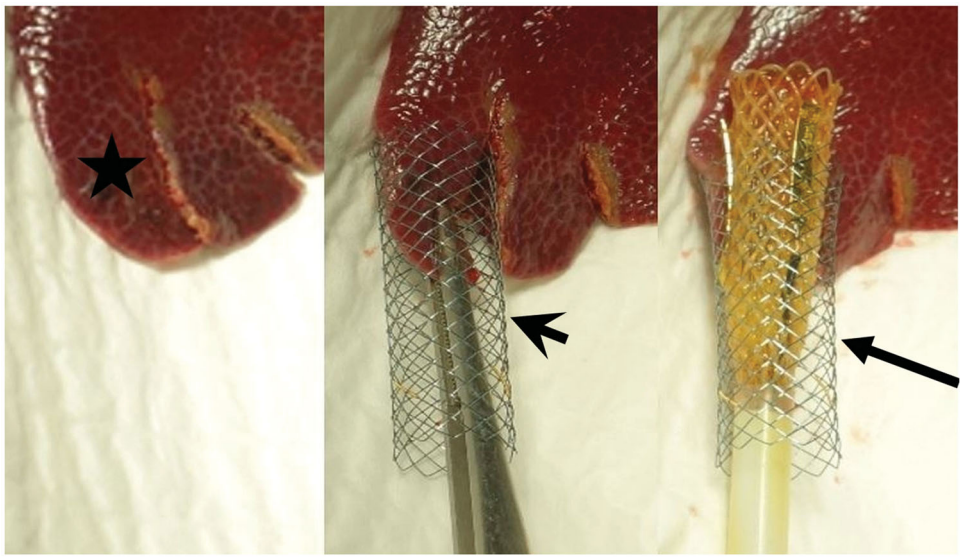

Figure 4. Demonstration of *in-vivo* liver bands (asterisk, left image) inserted into the metal stent (arrowhead, center image). A consequently inserted expandable tubular IRE catheter (arrow) is noted between the liver band and metal stent was (right image).

Monitoring of thermal effects

Heating of the stents and of surrounding liver tissue from the IRE application was monitored by the infrared camera (Workswell WIC 640; Workswell s.r.o., Czech Republic), which was fixed to a tripod 100 ± 20 cm from the observed subject. The temperature was measured in selected infrared images in the stent grooves before IRE and immediately after IRE (as stents were immediately extracted from the groove after IRE).

In vivo experiments

Experiments were performed under the supervision of the animal care staff of University of XXXX [partial redaction to maintain the integrity of review process], with prior approval for the use of animal test subjects from the Ethics Committee of the [partial redaction to maintain the integrity of review process], according to laws on the protection of animals against cruelty (as amended by §17, paragraph 15 g, Act no. 246/1992 Coll.).

Three laboratory female piglets, (50% Duroc, 25% Pietrain, and 25% Landrace cross-breed) were prepared as described in Appendix A. Shortly, the lower edge of the liver segment S3 was cut into strips 3 ± 1mm thick with preservation of their viability by maintaining their attachment to the central portion of the liver. All strips were inserted one by one into metal stents followed by insertion of the expandable endoluminal catheter (Figure 4). IRE application was performed with the same specified parameters as for the *ex vivo* study in 14 of these ingrowth models for scenarios A and B (single and double active electrodes in contact with inserted liver tissue). The remaining 13 strips were subject to similar procedure treatment without IRE application and were used as controls. Values of electric current, resistance, and power, as well as alterations in monitored vital functions, were measured for all experimental scenarios.

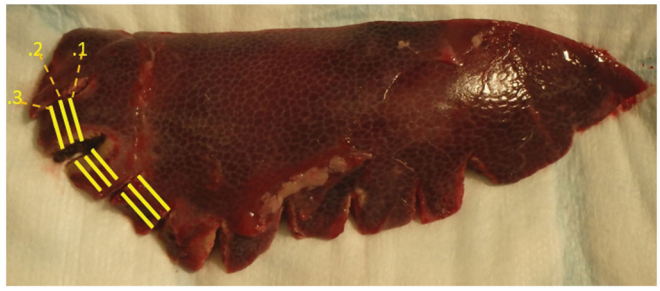

Figure 5. Histopathologic specimen immediately after section, with visualized liver bands cut perpendicular to the lower edge of the liver specimen. Yellow lines represent section for histopathological analyses at discrete distances from the lower edge of the liver. Each segment was further cut into 3 parallel slices and stained with haematoxylin-eosin.

All 3 pigs underwent control CT imaging (CT, GE Healthcare, USA, native examination, arterial and portal-venous phase after i.v. contrast injection [60 ml, Iomeron 300 – Iomeprol, Bracco International]) 2 h and 24 h after the procedure to exclude major complications such as abdominal bleeding, liver ischemia, liver hematoma, etc.

Histopathological analysis

All 3 animals were sacrificed and subsequently sampled 72 h after the procedure, as this represents the optimal time for evaluation of the viability of the liver strips at a time that IRE changes still persist [24,25]. Liver samples were fixed in a formaldehyde solution. Each liver strip was perpendicularly cut into three histological samples with varying distance from the lower edge of the liver (Figure 5). These portions were further cut into 3 slices parallel to the previous incision (each liver strip was finally divided into 9 samples on 3 slides). Samples were stained with hematoxylin-eosin for histopathological analysis to evaluate the presence, localization, and extent of necrosis, as well as the extent of inflammatory reaction and microscopic hemorrhage. Because of IRE-specific electrical gradient inhomogeneities in this environment and

Table 1. Differences in average resistance in relation to operating voltage and experimental scenarios.

Voltage	Scenario A resistance (Ω) Mean ± SD Median (95 % CI)	Scenario B resistance (Ω) Mean ± SD Median (95 % CI)	*p*-Value (Mann–Whitney)
300, 650, 1000	184 ± 34 183 (130; 230)	95 ± 23 96 (62; 133)	<0.001
300	212 ± 23 217 (180; 240)	110 ± 20 106 (79; 152)	<0.001
650	190 ± 22 198 (160; 222)	97 ± 15 98 (66; 120)	<0.001
1000	152 ± 27 160 (111; 183)	75 ± 12 75 (60; 95)	<0.001

Scenario A – double electrode contact; scenario B – single electrode contact.

Table 2. Differences in average current in relation to operating voltage and experimental scenarios.

Voltage	Scenario A current (A) Mean ± SD Median (95% CI)	Scenario B current (A) Mean ± SD Median (95% CI)	*p*-Value (Mann–Whitney)
300	1.1 ± 0.4 1.0 (1.0; 2.0)	2.0 ± 0.5 2.0 (1.0; 3.0)	0.006
650	3.1 ± 0.7 3.0 (2.0; 4)	6.3 ± 1.3 6.0 (5.0; 9.0)	<0.001
1000	6.0 ± 1.1 6.0 (5.0; 8.0)	12.6 ± 1.6 12.0 (10.0; 15.0)	<0.001

Scenario A – double electrode contact; scenario B – single electrode contact.

the resultant patchy appearance of necrosis at lower voltages, the extent of necrosis was evaluated semi-quantitatively (0 – no necrosis, 1 – minimal necrosis/< 5% of the sample, 2 – slight necrosis/5–25% of the sample, 3 – medium necrosis/25–50% of the sample, and 4 – extensive necrosis >50% of the sample).

Statistics

Data analysis was performed using Statistica (version 13). Multiple comparisons were made using one-way and two-way ANOVA test, followed by Mann–Whitney for dedicated paired examinations. For correlations, the Spearman correlation coefficient was used. To demonstrate the sensitivity and specificity of selected parameters a ROC curve was utilized. Statistical significance was defined as $p < 0.05$.

Results

Feasibility of IRE application in metal stents ex-vivo

At 300 and 650 V IRE application, all four scenarios were successfully completed as intended. At 1000 V, Scenario A ('double electrode contact') was successful for all attempts. Yet, short-circuiting occurred at 1000 V in all cases of in-stent ablation without interposed tissue (scenario C – stent mesh contact) and in two out of ten cases (20%) in scenario B (one electrode contact), as the electric current limit (50 A) of the IRE generator was reached. At 1300 V, only one case of scenario A was successfully completed (33%). At 1300 V, for all other scenarios short-circuit occurred in the metal stent immediately after initiation of IRE, preventing completion of energy application.

Prediction of the relation between stent and IRE electrodes ex vivo

Substantial differences for the values of electric current and resistance between single and double contact (Scenarios A & B) were observed at 300 V (217 vs 106 Ω, $p < 0.001$; and 1.0 vs 2.0 A, $p = 0.006$), 650 V (198 vs 98 Ω, $p < 0.001$; and 3.0 vs 6.0 A, $p < 0.001$), and 1000 V (160 vs 75 Ω, $p < 0.001$; and 6.0 vs 12.6 A, $p < 0.001$) (Mann–Whitney and Kruskal–Wallis ANOVA test). The results are summarized in Tables 1 and 2.

A cut off value of 130 Ω allowed indirect estimation of both the position of the active electrodes of IRE catheter within the occluded metal stent and determination as to whether one or two electrodes was delivering energy with a sensitivity of 95.2% (95% CI: 76.2–99.9%) and specificity of 92.9% (95% CI: 76.5–99.1%), AUC 0.986.

In scenario C, a stable very low resistance of 23 Ω at 300 and 650 volts was observed.

In scenario D, the average resistance of 176 ± 5 at 300 V, 167 ± 5 at 650 V, 166 ± 4 at 1000 V and 155 ± 4 at 1300 V were observed.

Thermal changes after IRE procedure in ex vivo settings

For both scenarios A and B (double and single electrode contact), thermal changes were nearly identical. The median temperature increase for these groups combined from the baseline temperature (21.9 ± 0.9 °C) was 0.9 °C at 300 V, 2.7 °C at 650 V, and 5.9 °C at 1000 V. These changes due to increasing voltage, however, were significant (300 V vs 650 V, $p < 0.001$; 650 V vs 1000 V, $p = 0.012$; Mann–Whitney test). A dramatic temperature increase of 20.3 °C was observed in the single successful 1300 V procedure from scenario A. This was associated with macroscopically visible coagulation

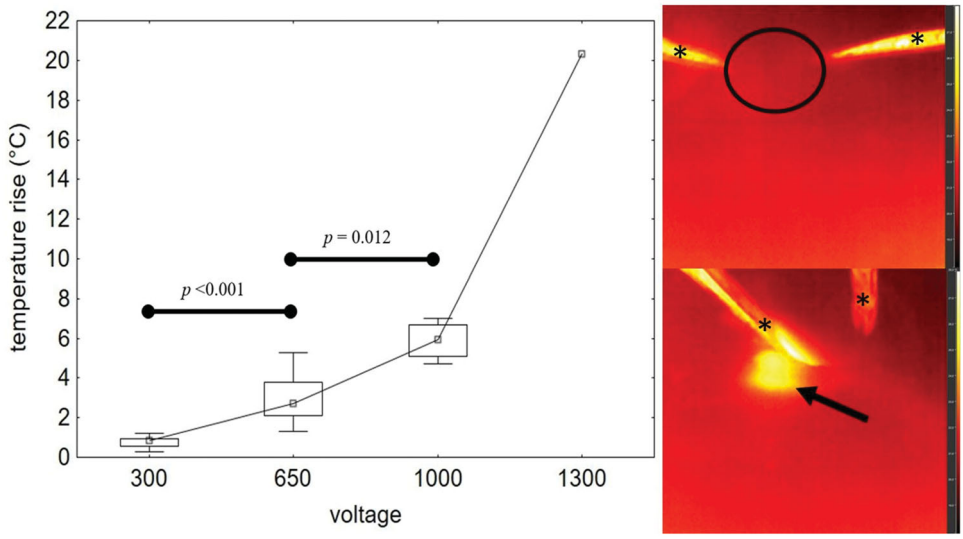

Figure 6. Left – graph demonstrating temperature rise during the IRE procedure in relation to voltage (scenarios A and B together), marked increase of measured temperature was recorded at 650 and 1000 V. Right – thermographic images demonstrating thermal changes before (up) and after (down) ablation in liver tissue surrounding the IRE catheter: scenario A, 1000 V, temperature increase from basal temperature 21.2 °C (circle) to 27.8 °C (arrow) immediately after ablation. Thermographic scale 18.0 °C to 28.0 °C. *Represent surgical tweezers.

changes. No macroscopic coagulation changes were visible in any other scenario. Temperature changes are visualized in Figure 6.

Feasibility of IRE in metal stent in vivo

In total, 14 IRE procedures were performed (8 scenario B and 6 scenario A), with 13 liver tissue bands left as controls. All IRE pulses in scenario A were delivered successfully at 650 and 1000 V. Early termination of the IRE occurred because of short-circuiting in three cases (37.5%) of the single contact scenario B (once at 650 V and in two attempts at 1000 V). This was associated with a dynamic drop of resistance during IRE resulting in the generator current limit being exceeded. During IRE, a 9% increase of the current was observed at 300 V, 19% at 650 V and 17% at 1000 V when comparing the initial and the end of session pulses. Detailed results are summarized in Table 3. No complications during the procedure and on follow-up CT examinations were observed.

Histopathological changes of IRE in vivo related to IRE settings

Histopathological analysis revealed necrotic changes in 9 of 14 IRE procedures (64.3%), roughly in proportion to applied voltage and amperage. The most extensive necrotic areas were observed in scenario B (single electrode contact) at 650 V and in scenario A (double electrode contact) at 1000 V (Table 4, Figure 7). The extent of histopathologic necrotic changes increased with applied voltage, when the necrosis was present at 300 V in one of three (33%) cases, at 650 V in 4 of 7 cases (57%) and 1000 V in all four cases despite early termination in two of them. Correlation between current and semiquantitative extent of necrosis was observed ($r^2 = 0.39$; $y = 3.27 + 0.95x$). No necrosis was observed histopathologically in any of the control samples, as only microscopic hemorrhage < 50% of the sample and minimal or no hepatic cellular changes such as nuclear atypia or inflammatory changes were present.

Table 3. IRE settings, completeness of the procedure, and measured current *in vivo*.

Voltage (V)	Scenario	Early termination	Average current (A)
300	B	No	3.0
300	B	No	2.0
300	B	No	2.0
650	A	No	5.0
650	A	No	4.0
650	A	No	2.0
650	A	No	3.8
650	B	No	5.3
650	B	No	5.0
650	B	After 20 s	6.0
1000	A	No	6.0
1000	A	No	8.0
1000	B	After 30 s	8.0
1000	B	After 70 s	6.5

Table 4. Summary of histopathological findings in relation to experimental scenarios and voltage of IRE.

Voltage (V)	Scenario	Necrotic changes
300	A	Not tested
300	B	No or very subtle (0–1)
650	A	Subtle to moderate (1–2)
650	B	Moderate to severe (2–4)
1000	A	Moderate to severe (2–4)
1000	B	Early termination after 30 and 70 s, subtle to moderate necrosis (1–2)

Discussion

This experimental study demonstrates the feasibility of performing endoluminal IRE in metal stents via an expandable tubular catheter. Electrodes mounted on a balloon catheter can overcome the size mismatch between the lumen of the stent and biliary tree and the much smaller size of a needle electrode tip routinely used for percutaneous ablations. In

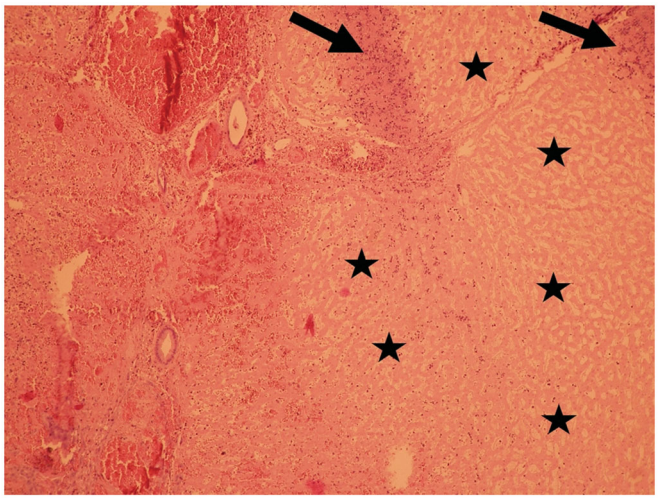

Figure 7. Histopathological analysis image (H-E staining) from Scenario B at 650 V demonstrating extensive necrosis (asterisk, right part of the image) surrounded by inflammatory cells (arrows). An uninjured bile duct and liver vein are visible in the right part of the image.

intraluminal IRE ablation of occluded or partially occluded metal stents, positioning of the IRE catheter is crucial. For a successful treatment effect, at least one of the electrodes must be in contact with the ingrowth tissue. Moreover, this study demonstrated that resistance and electric current values during IRE are different based upon the number of active electrodes (i.e., a calculated resistance of 111–240 Ω vs 60–152 Ω, and electric current of 2.0–12.6 A vs 1.1–6.0 A) when comparing double electrode and single electrode contact, respectively. This enables one to determine the number of active electrodes in contact with the stent with a sensitivity of 95.2% and specificity of 92.9%. The resistance values needed to estimate the position of the stent and electrodes can be obtained by several initial low voltage IRE pulses (e.g., 300 V). Resistance values from different positions of the IRE catheter and metal stent can indicate whether the occlusion covers the entire stent circumference or not. Thus, based on the resistance values it is possible to estimate which electrode is in contact with the metal stent and when it is no longer necessary to continue to electroporate.

The calculation of local resistance and modification of generator electric settings based on the number of active electrodes in contact with stent mesh is crucial for the selection of optimal ablation protocol and successful IRE. When the active electrode of an IRE catheter is in contact with the stent (scenario B), the stent itself can become an active electrode [21]. Given a much larger metallic surface area, this leads to significantly lower resistance calculated in this scenario (approximately half values compared to scenario A). When this event occurs, it is presumed that the IRE gradient is dependent on the distance between the other active electrode and the metal stent (corresponding to the thickness of interposed tissue) and if appropriate parameters are set, IRE is leading to the desired therapeutic effect. Accordingly, for scenario A, when two electrodes are in contact with interposed tissue, the distance between the active electrodes may be variable depending on the dilation of the tubular catheter to which the electrodes are attached. The narrower the stenosis, the less dilated the tubular catheter, and the smaller the distance between IRE electrodes, thus generating a larger IRE gradient between the electrodes and more extensive IRE changes. The electroporation will occur predominantly in the proximity of the active electrodes. In practice, it will be necessary to perform multiple electroporations for the treatment of the entire circumference of the stent.

We further observed situations where the current dropped below the threshold of the IRE generator resulting in the early termination of the IRE application. For example, IRE at 1000 V and higher voltages under conditions of very low calculated resistance (23 Ω) led to the termination of the process with currently more than 50 A. This can be explained by a rapid local decrease in resistance during the IRE and the formation of a permanent conductive channel in the tissue which lost its insulating properties.

IRE treatment in the proximity of the biliary tract has been reported with mixed results [26,27]. Endoluminal catheter-directed IRE was successfully applied in the porcine common bile duct with no adverse events [26], on the other hand, some studies show potential damage of biliary duct with stricture formation, whether IRE was applied endoluminaly or by direct needle placement [28,29]. Similar results were presented in studies using endoluminal treatment of porcine ureter [27]. However, this stricture formation may not be applicable when IRE ablation is performed inside the metal stent.

In 2016, Scheffer et al. experimentally analyzed the influence of metal stents on percutaneous liver IRE. They did not observe excessive heat production in the proximity to the metal stent both *in vitro* and *in vivo* swine model [19]. In our experimental usage of IRE for treatment of metal stent occlusion, the stent itself is considered as a protective device for adjacent tissue (Faraday cage principle) and the effect of IRE is limited to the lumen of the stent. In the *ex vivo* experiment, only a small change in temperature was observed at voltages up to 1000 V, which shows potential safety as well.

This study has several limitations. We were unable to estimate the full extent of IRE electrical field distribution, resultant ablation, or the thickness of the pathological tissue causing stent occlusion. In this pilot study, we did not study additional clinically relevant tissues such as tumor or mucosal hyperplasia and the effects of IRE were not compared with contemporary endoluminal ablation methods.

Thermal changes during endoluminal IRE were monitored only in the *ex-vivo* part of the experiment at room temperature. Endoluminal temperature measurement during IRE *in vivo* is technically challenging. However, thermal changes can be expected to be lower than *ex vivo* due to organ perfusion. Significant temperature increase typical for RF ablation was reached only in very high voltage settings, yet this fact must be taken into account in future studies and simulations.

Future studies should consider using higher IRE voltages (at least 650 V), include electrical current mathematical simulation [30] and try a more clinically relevant model of biliary metal stent occlusion than normal liver parenchyma. Extensive studies based on tissue models with different

thickness, homogeneity and impedance are needed to elucidate different tissue properties during IRE ablation. Future studies may also investigate clinically applicable protocol of endoluminal IRE ablation and compare the efficacy of IRE with other endoluminal ablation methods. For example, the ablation protocol currently under development can be based on fast pulse switching between electrode pairs of the 3-electrode tubular catheter and automatic selection of the most suitable voltage based on actual resistance measurements.

In conclusion, endoluminal IRE using an expandable tubular catheter in simulated metal stent occlusion is feasible under specific conditions. Based on *in vivo* models, optimal parameters for intraluminal IRE ablation for clearance of metal stents range between 650 and 1000 V. Resistance values calculated during IRE correspond to the number of active electrodes in contact with the metal stent mesh and ingrowth tissue. With further validation, this paradigm of clearance of a metal stent using IRE which we have initially explored for biliary stents occlusion may be expanded for more general use to treat metal stent occlusions in other organ systems.

Ethical approval

All applicable international, national, and institutional guidelines for the care and use of animals were followed. All procedures performed in studies involving animals were in accordance with the ethical standards of the institution or practice at which the studies were conducted.

Disclosure statement

S. Nahum Goldberg is a Consultant to Angiodynamics, Inc. and Cosman Medical, Inc. This research work has been carried out in the Center for Research and Utilization of Renewable Energy (CVVOZE).

Funding

This work was financially supported by the Ministry of Health of the Czech Republic [15-32484a and NU21-08-00561], Ministry of Health Specific Research Project of Masaryk University [MUNI/A/1488/2019], Ministry of Education, Youth and Sports under institutional support and BUT Specific Research Programme (project No. FEKT-S-20-6379) and Programme for Conceptual Development of Research Organization [FNBr, 65269705].

ORCID

T. Rohan http://orcid.org/0000-0002-7105-583X
T. Andrasina http://orcid.org/0000-0001-5723-5175
T. Juza http://orcid.org/0000-0003-0772-2287
P. Matkulcik http://orcid.org/0000-0001-7428-1202
D. Červinka http://orcid.org/0000-0001-7234-8805
V. Novotná http://orcid.org/0000-0003-0408-2771
V. Valek http://orcid.org/0000-0002-1593-0142
S. Nahum Goldberg http://orcid.org/0000-0003-2940-9822

References

[1] Andrašina T, Válek V, Pánek J, et al. Multimodal oncological therapy comprising stents, brachytherapy, and regional chemotherapy for cholangiocarcinoma. Gut Liver. 2010;4(1):S82–S88.

[2] Seidensticker R, Seidensticker M, Doegen K, et al. Extensive use of interventional therapies improves survival in unresectable or recurrent intrahepatic cholangiocarcinoma. Gastroenterol Res Pract. 2016;2016:e8732521.

[3] Rerknimitr R, Angsuwatcharakon P, Ratanachu-Ek T, et al. Asia-Pacific consensus recommendations for endoscopic and interventional management of hilar cholangiocarcinoma. J Gastroenterol Hepatol. 2013;28(4):593–607.

[4] Mizandari M, Pai M, Xi F, et al. Percutaneous intraductal radiofrequency ablation is a safe treatment for malignant biliary obstruction: feasibility and early results. Cardiovasc Intervent Radiol. 2013;36(3):814–819.

[5] Pai M, Valek V, Tomas A, et al. Percutaneous intraductal radiofrequency ablation for clearance of occluded metal stent in malignant biliary obstruction: feasibility and early results. Cardiovasc Intervent Radiol. 2014;37(1):235–240.

[6] Wu T-T, Li H-C, Li W-M, et al. Percutaneous intraluminal radiofrequency ablation for malignant extrahepatic biliary obstruction: a safe and feasible method. Dig Dis Sci. 2015;60(7):2158–2163.

[7] Kaassis M, Boyer J, Dumas R, et al. Plastic or metal stents for malignant stricture of the common bile duct? Results of a randomized prospective study. Gastrointestinal Endoscopy. 2003;57(2):178–182.

[8] Shah T, Desai S, Haque M, et al. Management of occluded metal stents in malignant biliary obstruction: similar outcomes with second metal stents compared to plastic stents. Dig Dis Sci. 2012;57(11):2765–2773.

[9] Tham T, Carr-Locke D, Vandervoort J, et al. Management of occluded biliary wallstents. Gut. 1998;42(5):703–707.

[10] Xu X, Li J, Wu J, et al. A systematic review and meta-analysis of intraluminal brachytherapy versus stent alone in the treatment of malignant obstructive jaundice. Cardiovasc Intervent Radiol. 2018;41(2):206–217.

[11] Cho JH, Jeon TJ, Park JY, et al. Comparison of outcomes among secondary covered metallic, uncovered metallic, and plastic biliary stents in treating occluded primary metallic stents in malignant distal biliary obstruction. Surg Endosc. 2011;25(2):475–482.

[12] Xia N, Gong J, Lu J, et al. Percutaneous intraductal radiofrequency ablation for treatment of biliary stent occlusion: a preliminary result. World J Gastroenterol. 2017;23(10):1851–1856.

[13] Auriemma F, De Luca L, Bianchetti M, et al. Radiofrequency and malignant biliary strictures: an update. World J Gastrointest Endosc. 2019;11(2):95–102.

[14] Mizandari M, Kumar J, Pai M, et al. Interventional radiofrequency ablation: a promising therapeutic modality in the management of malignant biliary and pancreatic duct obstruction. J Cancer. 2018;9(4):629–637.

[15] Bernard V, Andrašína T, Mornstein V, et al. Radiofrequency tissue ablation inside of metal stent – a thermographic study. IRBM. 2014;35(3):164–169.

[16] Eller A, Schmid A, Schmidt J, et al. Local control of perivascular malignant liver lesions using percutaneous irreversible electroporation: initial experiences. Cardiovasc Intervent Radiol. 2015;38(1):152–159.

[17] Faroja M, Ahmed M, Appelbaum L, et al. Irreversible electroporation ablation: is all the damage nonthermal? Radiology. 2013;266(2):462–470.

[18] Ben-David E, Appelbaum L, Sosna J, et al. Characterization of irreversible electroporation ablation in in vivo porcine liver. Am J Roentgenol. 2012;198(1):W62–W68.

[19] Scheffer HJ, Vogel JA, van den Bos W, et al. The influence of a metal stent on the distribution of thermal energy during irreversible electroporation. PLoS One. 2016;11(2):e0148457.

[20] Månsson C, Nilsson A, Karlson B-M. Severe complications with irreversible electroporation of the pancreas in the presence of a metallic stent: a warning of a procedure that never should be performed. Acta Radiol Short Rep. 2014;3(11):2047981614556409.

[21] Bernard V, Andrašina T, Červinka D, et al. A thermographic comparison of irreversible electroporation and radiofrequency ablation. IRBM. 2017;38(1):26–33.

[22] Appelbaum L, Ben-David E, Faroja M, et al. Irreversible electroporation ablation: creation of large-volume ablation zones in in vivo porcine liver with four-electrode arrays. Radiology. 2014;270(2):416–424.

[23] Rubinsky B, Onik G, Mikus P. Irreversible electroporation: a new ablation modality-clinical implications. Technol Cancer Res Treat. 2007;6(1):37–48.

[24] Andrašina T, Grolich T, Crha M, et al. The methodology for endoluminal irreversible electroporation in porcine models. Acta Vet Brno. 2019;88(2):201–205.

[25] Lee EW, Chen C, Prieto VE, et al. Advanced hepatic ablation technique for creating complete cell death: irreversible electroporation. Radiology. 2010;255(2):426–433.

[26] Ueshima E, Schattner M, Mendelsohn R, et al. Transmural ablation of the normal porcine common bile duct with catheter-directed irreversible electroporation is feasible and does not affect duct patency. Gastrointestinal Endosc. 2018;87(1):300.e1–300–e6.

[27] Srimathveeravalli G, Silk M, Wimmer T, et al. Feasibility of catheter-directed intraluminal irreversible electroporation of porcine ureter and acute outcomes in response to increasing energy delivery. J Vasc Interv Radiol. 2015;26(7):1059–1066.

[28] Andrasina T, Panek J, Cervinka D, et al. Irreversible electroporation for treatment of metal stent occlusion in biliary tract – ex vivo experimental model. CIRSE 2018 Abstrakt book [Internet]. Lisbon (Portugal): Cardiovascular and Interventional Radiological Society of Europe; 2018. [cited 2020 July 20]. Available from: https://link.springer.com/content/pdf/10.1007/s00270-018-2021-1.pdf

[29] Choi JW, Lu DSK, Osuagwu F, et al. Assessment of chronological effects of irreversible electroporation on hilar bile ducts in a porcine model. Cardiovasc Intervent Radiol. 2014;37(1):224–230.

[30] Miklavcic D, Sel D, Cukjati D, et al. Sequential finite element model of tissue electropermeabilisation. IEEE Transact Biomed Eng. 2005;52(5):816–827.